Weak Magnetic Field Measurement System

Andrés G. Delannoy

Office of Science, Summer Internship in Science and Technology Internship Program

University of Puerto Rico, Mayagüez

Fermi National Accelerator Laboratory

Batavia, Illinois

August 7, 2008

In partial fulfillment of the requirement of the Office of Science, Department of Energy's Summer Internship in Science and Technology Internship Program under the direction of Michael A. Tartaglia in the Technical Division at Fermi National Accelerator Laboratory.

Participant: _____

Signature

Supervisor: _____

Signature

Contents

ABSTRACT

Weak Magnetic Measurement System. ANDRES G. DELANNOY (University of Puerto Rico, Mayagüez, PR 00682) MICHAEL TARTAGLIA (Fermi National Accelerator Laboratory, Batavia, IL 60510)

This paper describes the research performed on a Hall probe based magnetic measurement system in order to determine if it is capable of recording magnetic fields of required magnitude generated by superconducting solenoid magnets. These superconducting solenoids are being developed for a R&D project named High Intensity Neutrino Source. The project design demands a very low stray field due to adjacent RF cavities. This paper presents the performance of a Hall probe based measurement system when excited by DC and AC currents. The probe's sensitivity to an external weak magnetic field was measured and an estimate of the electromagnetic noise level was performed. Various noise sources were studied and efforts made to attenuate them using software and hardware based signal recovery. The probe's sensitivity was found to vary in relation to the current applied. AC probe excitation was found to provide a lower noise level versus DC excitation.

1. INTRODUCTION

i. High Intensity Neutrino Source

The High Intensity Neutrino Source (previously known as Proton Driver) project proposes a 2 MW, 8 GeV, proton linear accelerator based on approximately 400 independently phased superconducting and room temperature resonators. The initial beam acceleration is achieved by using a Radio-Frequency Quadrupole (RFQ) (from 0.05 MeV to 2.5 MeV) and room-temperature (RT) accelerating cavities (up to ~10 MeV), each combined with a superconducting focusing solenoid [2, 9, 12].

The purpose of the HINS R&D program [13] is to address accelerator physics and technology questions for a new concept, low-energy, high intensity, long-pulse H^- superconducting linear accelerator. In particular, the goals of the program are to:

- Demonstrate beam acceleration using superconducting spoke-type cavity structures starting at a beam energy of 10 MeV
- Demonstrate the use of high power RF vector modulators to control multiple RF cavities driven by a single high power klystron for acceleration of a non-relativistic beam
- Demonstrate beam halo and emittance growth control by the use of solenoid focusing optics up to 60 MeV
- Demonstrate fast, 325 MHz bunch-by-bunch, beam chopper

ii. Magnetic Measurements

When operational, the HINS solenoids will be cooled down to 4.5 K with liquid helium, operate at 250 A, and have a maximum magnetic field strength of 7.5 T. Their design comprises

a main coil, two buckling coils, two dipole corrector windings, and a low carbon steel flux return. Some of the magnets will have horizontal and vertical corrector dipoles installed in the inner diameter of the solenoid coil. These solenoids are designated as Type-2. The addition of the dipole correction coils also adds two pairs of power leads to the cryostat, which are not present in Type-1 solenoids [2, 9, 12].

The magnetic tests are meant to verify model predictions and investigate measurement issues in general. Field strength and alignment issues are studied in particular. Some of the measured parameters include strength vs. axial position, central field strength and transfer function, and bipolar and unipolar hysteresis loops. Disagreement between model predictions and measured data can lead from calibration corrections to removal of ferromagnetic material in the measurement equipment [2].

The most common instrument used to measure magnetic field strength is the Hall probe. This probe relies on the Hall Effect to detect the presence of a magnetic field. Recall that moving charges are deflected by magnetic fields by the Lorentz Force,

$$(\boldsymbol{F} = q\boldsymbol{v} \times \boldsymbol{B}).$$

Consequently, current running through a conductor will tend to deposit charge in one end of the material, thus producing an electric field (see Figure 1). The magnitude of the magnetic field will be proportional to the potential difference across sides of the conductor opposite to the current flow.

Magnetic measurements are performed both at warm (300 K) and cold (4.2 K) temperatures. A low current is run through the magnet's windings at room temperature. The current must be very limited because the winding material is not a good conductor at room temperature. There is a small amount of copper in the winding material that helps carry this current. The electro-magnet in response generates a very weak magnetic field.

As part of the design requirements, the stray on the axis must be kept below 5×10^{-4} T at a distance of 150 mm from the center of the solenoid (which is its total length). These measurement conditions where the magnetic field has such a magnitude create a challenging measurement scheme. Electromagnetic noise and unwanted signals from a variety of sources will inevitably find its way and be recorded by the measurement system. There are sources of noise (such as Johnson noise, 1/f noise, and shot noise) which are due to fundamental processes and may not be eliminated. Since some of these sources have a 1/f spectrum – the noise amplitude increases as the frequency goes to zero – their effect will be worst at DC [1]. One of the efforts of this research was to develop a method of recovering the field strength signal from the ambient electromagnetic noise.

iii. LabVIEW

A first approach to signal recovery methods was to use software development. National Instrument's LabVIEW was used extensively to model noisy signals and filter them by various methods. LabVIEW (**Lab**oratory **V**irtual **I**nstrumentation **E**ngineering **W**orkbench) is a platform and development environment for a graphical programming language. It is commonly used for data acquisition, instrument control, and industrial automation. Execution is determined by the

structure of a graphical block diagram on which the programmer connects different function-nodes by drawing wires. These wires propagate variables and any node can execute as soon as all its input data become available.

LabVIEW programs/subroutines are called virtual instruments (VI). Each VI has three components: a block diagram, a front panel, and a connector pane. A VI can either be run as a program with the front panel serving as a user interface or, when dropped as a node onto the block diagram, the front panel defines the inputs and outputs for the given node through the connector pane. The graphical approach also allows non-programmers to build programs simply by dragging and dropping virtual representations of lab equipment with which they are already familiar [8].

iv. Lock-In Amplifier

The lock-in amplifier is a type of amplifier that can recover a modulated signal with a known frequency from extremely noisy environment. Operation of a lock-in amplifier relies on the orthogonality of sinusoidal functions. Specifically, when a sinusoidal function of frequency θ is multiplied by another sinusoidal function of frequency φ not equal to θ and integrated over a time much longer than the period of the two functions, the result is zero. In the case when φ is equal to θ, and the two functions are in phase, the average value is equal to half of the product of the amplitudes. Alternatively, we can see this with a simple trigonometric identity. The original noisy signal $(Acos\varphi)$, with unknown amplitude (A), is mixed with a reference signal $(2cos\theta)$ with a known amplitude (2) and frequency (θ):

$$(2cos\theta)(Acos\varphi) = Acos(\theta - \varphi) + Acos(\theta + \varphi).$$

If we can make our signal of interest periodic at some specific frequency, offset and drift will no longer be a concern. We can choose a frequency high enough to avoid 1/f noise, yet low enough to be "quasi-static" (to not materially affect the phenomena under study), and which is far from any significant noise source. The noisy signal is made to oscillate at the same frequency as the reference signal by making the reference signal act as a chopping signal. A square wave reference signal can be used to periodically interrupt the signal so that when both signals are mixed the noisy signal is rectified at the given reference signal frequency:

$$= A + Acos(2\theta), \text{ where } (\theta \approx \varphi).$$

A low-pass filter, consisting of a resistor in series and a capacitor in parallel, is then applied to the resulting signal, thereby getting rid of the double frequency term $(Acos2\theta)$. We finally obtain a non-oscillating signal with the magnitude of the original signal of interest (see Figure 2):

$$= A \quad (V_{DC}).$$

This lock-in amplifier model is capable of synchronous rectification of only half of the signal. For a signal recovery device such a waste of signal information would be unacceptable. Commercial lock-in amplifiers therefore include a full wave synchronous demodulator which usually works by using inverting and non-inverting amplifiers to produce anti-phase versions of the signal (i.e. 180° out of phase). Both the phased and anti-phased versions of the signal are chopped by the square wave reference signal. The anti-phased signal is inverted (multiplied by -1) before being recombined with the phased signal. The result is a fully rectified signal (shown in Figure 3) which is then filtered with a low-pass [1, 8, 10, 12].

2. MATERIALS & METHODS

i. LabVIEW Simulations

LabVIEW software by National Instruments was used to develop noise filtering software. Two main ideas were developed and tested. One idea was based on a lock-in amplifier and the other on curve fitting. Various lock-in models were developed based on simple schemes:

Square wave chopper + low-pass model [1]

This model behaves like the fully rectifying lock-in amplifier described in the introduction (Figures 2 & 3). A Signal Simulation VI is setup with a sine wave with uniform white noise. The frequency of this signal is specified and both the sine wave and white noise amplitude are controlled in the front panel (Figure 5) by a slider. This signal is then split and merged with two square wave chopper reference signals. The chopper signals share the original signal's frequency. One of the chopper signals is setup as the inverse of the other, and it is this inversed chopper signal which is merged with an inverse of the original signal.

Each of the resulting signals is independently filtered using a Low-Pass Filter VI operating close to the reference frequency. The two signals are then merged by applying a trigonometric identity through a Formula VI:

$$\sqrt{X^2 + Y^2} = \sqrt{A^2 sin^2\theta + A^2 cos^2\theta} = A$$

At this point the original signal's amplitude has been reconstructed and the result is plotted with a Graph VI. The numerical value of the amplitude is analyzed by an Amplitude and Level Measurements VI and a value of the peak to peak amplitude is returned by another Graph

VI and a Numerical Indicator VI. We can take the peak to peak amplitude of the signal as the actual amplitude because it is a rectified wave (see Figure 4).

Sinusoidal wave chopper + low-pass model [10]

This lock-in amplifier model differs from the former in that the chopper reference signals are sinusoidal waves $180°$ out of phase with each other. Also, the reconstructed peak to peak amplitude is averaged by a Statistics VI performing an arithmetic mean on the signal as shown in Figures 6 & 7.

Curve fitting model

This model attempts to apply a two-term curve fit to the input signal (see Figures 8 & 9). A Signal Simulation VI is setup with a sine wave with uniform white noise. A Curve Fitting VI applies a general least squares linear model to the input simulated data and returns the coefficient for the following models:

a0*(sin(2*3.14*10.1*x))

a1*(cos(2*3.14*10.1*x)).

The VI outputs the numerical value of coefficients a0 and a1. Here, the model reconstructs the signal assuming that it takes the form of a sinusoidal term with an angular frequency of

$\omega = 2\pi\theta$, where θ is the reference frequency.

The best fit is then plotted by a Graph VI and the peak to peak amplitude is calculated by an Amplitude and Measurements VI. The peak to peak amplitude is divided by two to calculate the wave's actual amplitude and its value is plotted by a Chart VI. The coefficients are returned

by an Array Indicator VI and the signal amplitude is finally determined by a Formula VI applying the equation:

$$\sqrt{X^2 + Y^2} = A, \text{ where } X = a_0 sin(2\pi * 10.1x) \text{ and } Y = a_1 cos(2\pi * 10.1x).$$

ii. Data Acquisition

A Hall probe based magnetic measurement system was studied with the goal of determining if the probe model HSP-T by Cryomagnetics is able to measure the magnitude of the magnetic field we demand for the HINS solenoids. The experimental goals were to measure the sensitivity of each probe to a change in the external magnetic field and to determine the noise level for several setups. Two of these probe models were mounted on the center of a plastic disk 12.5 cm in diameter. The probe on top of the disk was labeled as "1" and the one in the bottom as "2". BNC connectors for each probe's current excitation input and probe voltage output were mounted on an extension of the disk (see Figure 10). The probes were excited by alternating and direct current to determine the most effective measurement method.

Additionally, a two turn copper coil was wound around the edge of the disk and fastened to another extension on the disk. The current source used for driving the coil was Hewlett Packard's E3610A model (Figure 10). The measurement system was enclosed in a nested magnetic shield. This helped reduce the noise level before taking measurements. This setup resembled the real experimental setup, were the probe is shielded as well.

The data was read and digitalized using a PXI (**P**CI e**X**tensions for **I**nstrumentation) modular instrumentation platform. This particular model, National Instruments' PXI-1031 DC (Figure 12), housed three modules:

- PXI-8336 MXI-4 fiber optic – communicated the data to the PC
- PXI-GPIB – communicated with other instruments in GPIB interface
- PXI-6281 M-Series Multifunction DAQ – communicated with NI's model BNC-2110 (Figure 13)

All experimental data was recorded to file using LabVIEW. Essentially, a different and independent program was written for each experimental setup. LabVIEW's DAQ Assistant and Instrument I/O Assistant VI's were used extensively in data entry to file. The PXI ultimately read data from GPIB (General Purpose Interface Bus) instruments as well as analog voltage data. The Write to Measurement File VI was also used in every data recording code. Figure 14 shows two typical data recording programs. Also notable is the fact that these programs all had the number of samples determined by a "for" loop and the sample rate controlled by the Wait VI.

DC Probe Excitation (Figure 15)

The DC power supply used for probe excitation was Keithley's 2400 SourceMeter (Figure 16). It was set as a current source at 100 mA, in agreement with manufacturer's specifications [5] for nominal current in.

The probe voltage was processed through a Stanford Research System's SIM 911 BJT Preamp (Figure 17). This low-noise preamp increased the signal's amplitude by 100 times. Data was collected for two DC excitation setups: The amplified probe voltage was sent through a low-pass analog filter in one arrangement and recorded directly in the other. The analog filter was set up as a Butterworth filter with a 20 Hz cutoff frequency and 36 dB/oct.

For DC probe sensitivity and noise level studies the coil's current was ramped from 0 to 2.1 A, in 0.1 A steps, while the probe's excitation current was kept at a constant 100 mA. The probe response to the changing magnetic field was recorded as a voltage using the BNC-2110 DAQ. One thousand data points were recorded for each current step of the coil. The sample rate was set at 33 samples per second. The data recording code produced a text file with a column for the time at which the sample was recorded and a column for the value of the voltage in Volts. The data was dumped on a spreadsheet and analyzed in μVolts (also compensating for the pre-amp provoked increase in gain).

AC Probe Excitation (Figure 18)

For AC excitation, the alternating current was generated by the Signal Recovery's 7265 Lock-In Amplifier (Figure 19) as a reference signal. The AC source was based on a voltage setting, and was fixed at 5 V_{RMS} (the highest allowed setting) as would be done in the actual experiment. This alternating current was stepped down by a 10:1 transformer to match the manufacturer's specifications for nominal current input.

The probe voltage was input into and processed by the lock-in amplifier as discussed in section iv of the Introduction. The probe's response to the changing magnetic field was read and recorded through GPIB interface. Again, the coil's current was ramped from 0 to 2.1 A, in 0.1 A steps. One thousand data points were collected for each current step of the coil. The sample rate was set at 33 samples per second. The data recording code produced a text file with a column for the time at which the sample was recorded and a column for the value of the voltage in Volts. The data was dumped on a spreadsheet and analyzed in μVolts.

The reference signal's frequency was varied from 10 to 40 Hz for this study with expectations to find that the noise level would be markedly lower at one specific frequency. The data was collected and analyzed then for four data sets for each probe.

iii. Noise Sources Studies

AC Source Noise Frequency Response (Figure 20)

A study of the noise level at various frequencies was performed on the lock-in amplifier's reference signal. The AC signal was processed by the transformer and then used to excite the probe. The probe's voltage response was read and processed by the lock-in amplifier, and ultimately recorded via GPIB interface. The reference signal frequency was ramped from 10 to 120 Hz in 10 Hz steps. One thousand samples were recorded for each step, at a rate of 2 samples per second.

Transformer Operation versus Frequency (Figure 21)

The transformer's response to change in reference signal frequency was measured. The AC source was sent to the 10:1 transformer and immediately read and processed by the lock-in amplifier. Of course, the lock-in output showed a time-independent signal as the input signal was composed of just the reference signal. The same processed voltage was recorded but without the transformer in the setup. With both the transformer present and absent in the circuit, the reference signal frequency was ramped from 10 to 100 Hz in 10 Hz intervals. The constant voltage was read visually in the lock-in amplifier's display and confirmed by GPIB voltage measurement.

Coil Current Source Noise Analysis (Figure 22)

The noise contribution of the coil's current source was examined by comparing the displayed current and a measurement of the actual current output of the instrument. A 1.1 Ω shunt resistor was set in series to the current path to make current measurements possible. The current then drove the coil from 0 to 2.1 A (in 0.1 A steps) while voltage measurements were being taken in parallel to the resistor. One thousand data points were collected for each current step of the coil. The sample rate was set at 33 samples per second.

3. RESULTS

i. Hall Probe's Coil Magnetic Field Calculation

We assume a current of 1 Ampere running through a coil with a circular winding of 2 turns. We take the coil's diameter, $2a$, as 12.5 cm.

From the Biot and Savart Law[4, 6, 11]:

$$\boldsymbol{B}(\boldsymbol{r}_2) = \frac{\mu_0}{4\pi}\int \frac{\boldsymbol{I}\times(\boldsymbol{r}_2-\boldsymbol{r}_1)}{|\boldsymbol{r}_2-\boldsymbol{r}_1|^3}$$

$$\boldsymbol{B}(\boldsymbol{r}_2) = \frac{\mu_0}{4\pi} I\int \frac{d\boldsymbol{l}\times(\boldsymbol{r}_2-\boldsymbol{r}_1)}{|\boldsymbol{r}_2-\boldsymbol{r}_1|^3}$$

Where $\boldsymbol{I} = Id\boldsymbol{l}$ is the current through the coil, $\boldsymbol{r}_1$ is the source charge vector, $\boldsymbol{r}_2$ is the field or probe point vector, and $\mu_0 = 4\pi\times 10^{-7}\frac{N}{A^2}$. See Figure 23.

$$d\boldsymbol{l}\times(\boldsymbol{r}_2-\boldsymbol{r}_1) = |d\boldsymbol{l}||\boldsymbol{r}_2-\boldsymbol{r}_1|sin\left(\frac{\pi}{2}\right) = |d\boldsymbol{l}||\boldsymbol{r}_2-\boldsymbol{r}_1|$$

$$B(\boldsymbol{r}_2) = \frac{\mu_0}{4\pi} I\int_0^{4\pi}\frac{|d\boldsymbol{l}||\boldsymbol{r}_2-\boldsymbol{r}_1|}{|\boldsymbol{r}_2-\boldsymbol{r}_1|^3} = \frac{\mu_0}{4\pi} I\int_0^{4\pi}\frac{|d\boldsymbol{l}|}{|\boldsymbol{r}_2-\boldsymbol{r}_1|^2}$$

$$\{|d\boldsymbol{l}| = ad\theta\}$$

$$\left\{|\boldsymbol{r}_2-\boldsymbol{r}_1| = \sqrt{z^2+a^2}\right\}$$

$$B(\boldsymbol{r}_2) = \frac{\mu_0}{4\pi} I\int_0^{4\pi}\frac{ad\theta}{z^2+a^2}$$

Since the polar angle and the radius are constant for the coil, the horizontal components of the magnetic field cancel. The vertical component corresponds to the cosine of the angle the z-axis makes with vector $d\boldsymbol{l} \times (\boldsymbol{r}_2 - \boldsymbol{r}_1)$. This quantity equals $\left(\frac{a}{|\boldsymbol{r}_2 - \boldsymbol{r}_1|}\right)$.

$$\left\{\boldsymbol{B}(\boldsymbol{r}_2) = B_z\hat{\boldsymbol{z}} = \left[\left(\frac{a}{|\boldsymbol{r}_2 - \boldsymbol{r}_1|}\right)B(\boldsymbol{r}_2)\right]\hat{\boldsymbol{z}} = \left[\left(\frac{a}{\sqrt{z^2 + a^2}}\right)B(\boldsymbol{r}_2)\right]\hat{\boldsymbol{z}}\right\}$$

$$\boldsymbol{B}(\boldsymbol{r}_2) = \frac{\mu_0}{4\pi} I \frac{a^2}{(z^2 + a^2)^{\frac{3}{2}}}\hat{\boldsymbol{z}} \int_0^{4\pi} d\theta$$

$$\boldsymbol{B}(\boldsymbol{r}_2) = \mu_0 I \frac{a^2}{(z^2 + a^2)^{\frac{3}{2}}}\hat{\boldsymbol{z}}$$

Taking $z = 0$, in order to find the field at the axis of the coil, we find:

$$\boldsymbol{B}(z = 0) = \frac{\mu_0 I}{a}\hat{\boldsymbol{z}}$$

For a current of 1A we have:

$$\boldsymbol{B}(z = 0, I = 1A) = \frac{\left(4\pi \times 10^{-7}\frac{N}{A^2}\right)(1\ A)}{\frac{1}{2}(.125\ m)}\hat{\boldsymbol{z}} = 2.0106 \times 10^{-5}\ \frac{N}{A - m}\left|\frac{10^4\ G}{\frac{N}{A - m}}\right|\hat{\boldsymbol{z}}$$

$$\boldsymbol{B} = .20106\ G\ \hat{\boldsymbol{z}}$$

Therefore 0.20106 Gauss will be generated per Ampere. So our transfer function for the coil is then

$$\boldsymbol{B}(\boldsymbol{r}_2) = \frac{\mu_0 I}{a}\hat{\boldsymbol{z}}$$

or $0.20106\ \frac{G}{A}$ (given the constant disk diameter and probe position on disk surface).

ii. DC Probe Excitation

DC sensitivity and noise level analysis with no filter

The arithmetic mean,

$$\bar{x} = \frac{1}{n}\sum_{i=1}^{n} x_i,$$

of the one thousand samples was calculated for each step in the current ramp. A linear fit was performed on a plot of these averages versus the magnetic field being generated by the coil at that particular coil current (Figures 24 & 25). This magnetic field was calculated using the transfer function calculation shown above.

The linear fit provided the slope of the curve which determined the sensitivity of the probe for this specific probe excitation method. The sensitivity describes the change in voltage across the Hall probe with respect to a change in the external field.

Two kinds of noise analysis were carried out with the collected data. One kind of noise level was calculated from the data's deviation from linear behavior. Residuals,

$$R = y_i - f(x_i, a_1, \ldots, a_n),$$

were computed from the difference in the averaged values and the linear fit values. The standard deviation,

$$\sigma = \sqrt{\frac{1}{N}\sum_{i=1}^{N}(x_{i\_}\bar{x})^2},$$

was calculated for this set of residuals. This value indicated the range of the noise level in terms of μV for the divergence from linear performance.

The other kind of noise level analysis worked out involved studying the range of value within the one thousand voltage samples. The current ramp step with the broadest spread was selected as a worst case and studied in detail. The standard mean error,

$$s_e = \frac{\sigma}{\sqrt{N}},$$

was computed as a measure of this spread in the samples.

Using the value of the probe's sensitivity, the noise level was expressed in terms of Gauss and allowed the determination of the excitation method's efficiency. The values of the sensitivities and noise levels for probe 1 and 2 are indicated in Table 1.

DC sensitivity and noise level analysis with filter (Figure 26)

The DC probe excitation studies and result analysis were duplicated, except that a Butterworth Filter was placed in the circuit after the low-noise pre-amp. The linear fits performed on the plots of voltage versus magnetic field generated are shown in Figures 27 & 28. The values of the sensitivities and noise levels for probe 1 and 2 are indicated in Table 1.

We can observe a clear reduction in noise as the low-pass filter is implemented. This reduction in noise not only allows a better signal recovery, but also makes the sensitivity

measurement more precise. The noise reduction decreases the noise level about an order of magnitude making the overall reduction in noise comparable to the lock-in amplifier. We also observe a disparity in the value of the sensitivity of the probes.

iii. AC Probe Excitation

The analysis for AC probe excitation was very similar to the DC study. The sensitivity plots were constructed in the same manner (Figures 29-36) and the noise analysis was identical. The results were very consistent through the range of frequency studied. The sensitivity measurements were very reproducible and the noise level was stable throughout. There was a noticeable difference in the value of the sensitivity compared to DC excitation. Also, the sensitivity values between both probes were again disparate.

iv. AC Source Noise Frequency Response

The investigations were conducted at different frequencies from 10 to 120 Hz, in an attempt to find an operational frequency with less background noise. A tendency for the noise to decrease with increasing frequency and a peak at 60 Hz was observed. These results motivate more thorough studies of the background noise at a broader range of frequencies. None of the tested frequencies offered an outstandingly lower noise level but the reference frequency may be increased until a satisfactory noise level is attained.

vi. Transformer Operation versus Frequency

The reference frequency was ramped from 10 to 100 Hz to measure the effect on the behavior of the transformer. A transparent instrument would be independent of the frequency. This was the case when the transformer was excluded from the setup. For the transformer in

the circuit, the measured voltage increased as reference frequency increased, reaching an almost constant value at about 70 Hz. This find also suggests setting the lock-in reference signal at a higher frequency.

vii. Coil Current Source Noise Analysis

The current running through the coil was carefully measured and compared to the displayed value by the current source. The response was a very linear behavior. After a standard error in the mean calculation for the worst of one thousand samples, a deviation of 0.003 A was computed. From this value the contribution to the noise level was calculated as $\frac{0.003\text{A}}{0.02\,\frac{\text{A}}{\text{G}}} = 0.00006\ \text{G}$. This level of noise is negligible compared to the background noise level and the instrument was ruled out as being a big contribution to the noise.

4. DISCUSSIONS & CONCLUSIONS

The software simulations developed in LabVIEW yielded results which depended on the signal to noise ratio for the original signal. For a 1:1 SNR the simulations returned a relative error of 5-10%. The results for AC noise frequency response show the largest background noise for probe 1 at around 200 μV. This equals a noise level of $\frac{200\ \mu\text{V}}{10\ \frac{\mu\text{V}}{\text{G}}} = 20\ \text{G}$ which is two orders of magnitude higher than our required measurement signal magnitude. At this SNR the LabVIEW simulations do not return stable values for the amplitude of the original signal. These simulations were thus abandoned and attempts were then focused on data acquisition.

From glancing at the results we can notice a discrepancy between the measured sensibility for probe 1 and 2. The possibility of this being caused by geometric inconsistencies was explored. A rough calculation of the change in magnetic field as the probe is displaced off-center was performed. This showed a very weak effect and it was concluded that the probes have different sensibilities due to variations between manufactured models.

A correlation that was discovered by analyzing the data was the sensitivity dependence on probe excitation current. Different values for the sensitivity of the same probe were observed when measuring with DC versus AC probe excitation (see Table 2). This disagreement is explained by the fact that the amount of current exciting the probe will have an effect on its sensitivity. AC excitation was not only a different excitation method, but the amount of current was different as compared to DC excitation.

The noise levels for DC excitation only compete with the AC excitation levels when a low-pass filter is applied. Even so, we can see a more consistent noise level measurement for

AC excitation. The lock-in amplifier allows us to reduce the noise to a 0.01G level and therefore probe down and measure the required field strength. The analysis made on the background AC noise level, the transformer, and coil power supply indicate that the noise level could be further reduced by using better magnetic shielding methods and higher precision equipment.

5. FUTURE WORK

- Calculate the exact change in magnetic field as probe is moved off-center.
- Perform detailed noise level analysis at wider range of frequencies for AC probe excitation.
- Study shielding methods & their effectiveness.
- Study cryogenic temperature measurements.

6. LITERATURE CITED

[1] Bentham Instruments Ltd. Lock-in Amplifiers. 225.02 Reading, Berkshire, England, 2002

[2] Carcagno R., et al. Superconducting Solenoid Magnet Test Results. ASC-06, Seattle, 2006.

[3] Carcagno R., et al. Test Solenoids: Expected Performance and Test Results. TD-06-027, TD-06-028, TD-06-029, FNAL, July 2006.

[4] Griffiths, David J. Introduction to Electrodynamics. 3rd ed. New Jersey: John Wiley & Sons, 1999 p.215-218.

[5] Hall Effect Sensors. Cryomagnetics, Inc. 7 Aug. 2008. http://www.cryomagnetics.com/hall-sensor.htm

[6] Jackson, John D. Classical Electrodynamics. 3rd ed. California: John Wiley & Sons, 1999 p.174-178.

[7] Kromer P., et. al. PC-Based Digital Lock-In Detection of Small Signals in the Presence of Noise. Department of Physics, University of Texas at Austin

[8] NI Labview – The Software That Powers Virtual Instrumentation. National Instruments Corporation. 7 Aug. 2008. http://www.ni.com/labview/

[9] Page, T., et. al. High Intensity Neutrino Source Superconducting Solenoid Cryostat Design. TD-07-360, FNAL, 2007

[10] PerkinElmer Instruments Inc. What is a Lock-in Amplifier? TN 1000. Tennessee, 2000

[11] Reitz, John R., and Frederick J. Milford. Foundations of Electromagnetic Theory. London: Addison Wesley, 1960 p.149-159.

[12] Terechkine I., et al. Focusing Solenoid for the Front End of a Linear RF Accelerator. PAQ-07, Albuquerque, 2007.

[13] Webber, B., High Intensity Neutrino Source R&D Program Goals Statement. Jan 2008

7. ACKNOWLEDGEMENTS

- Michael A. Tartaglia
- Dmitri A. Sergatskov
- Tom Page
- John Tompkins
- Guram Chlachidze
- Cosmore Sylvester
- Magnet Systems Department
- Melissa M. Ruiz
- U.S. Department of Energy
- Office of Sciene
- Fermi National Accelerator Laboratory

8. FIGURES & TABLES

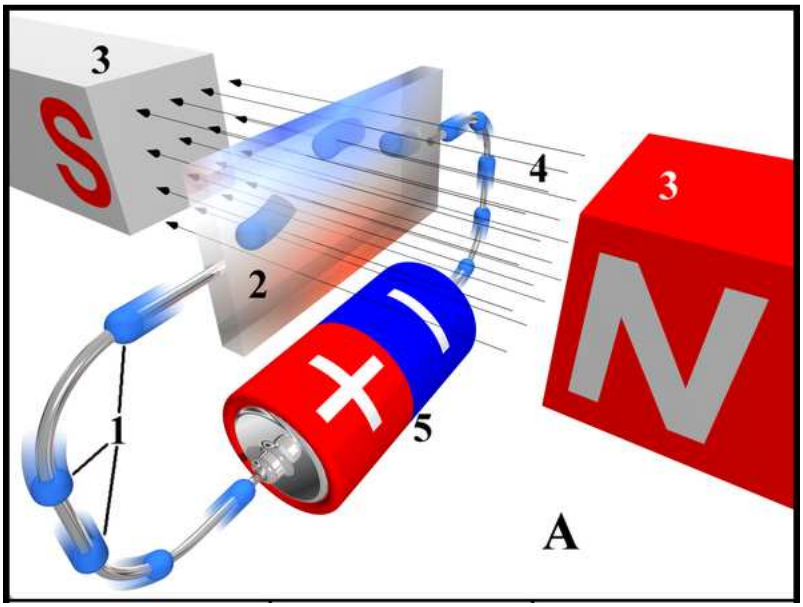

Figure 1: The Hall Effect. (1) Charge carriers. (2) Conducting plate. (3) Magnet. (4) Magnetic Field. (5) Voltage Source.

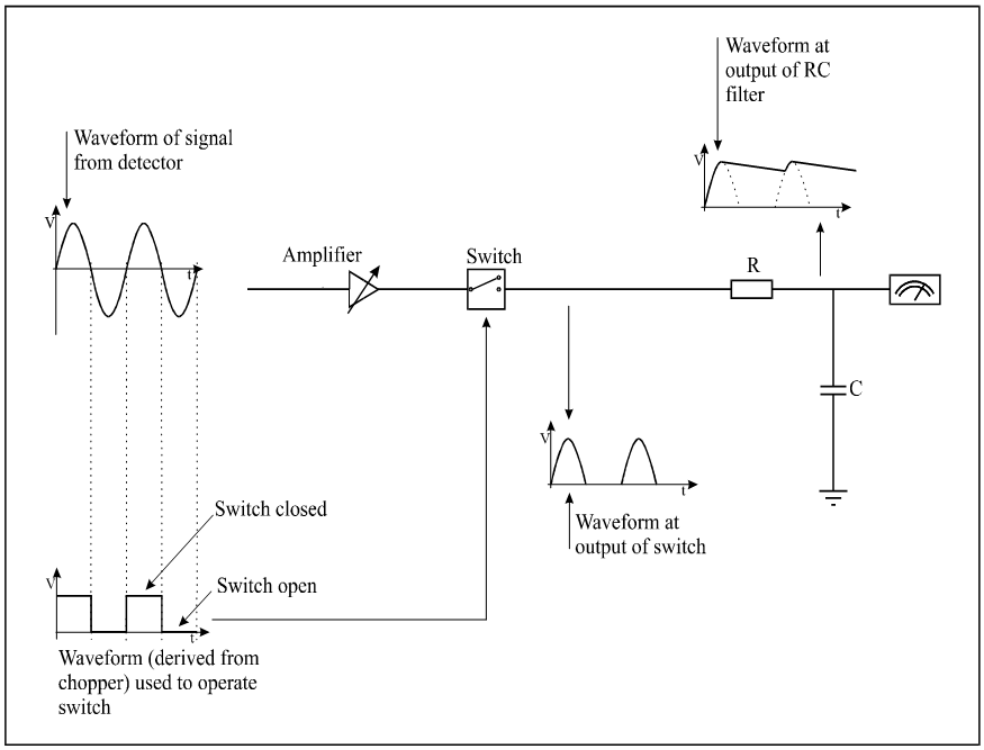

Figure 2: Simple lock-in amplifier model

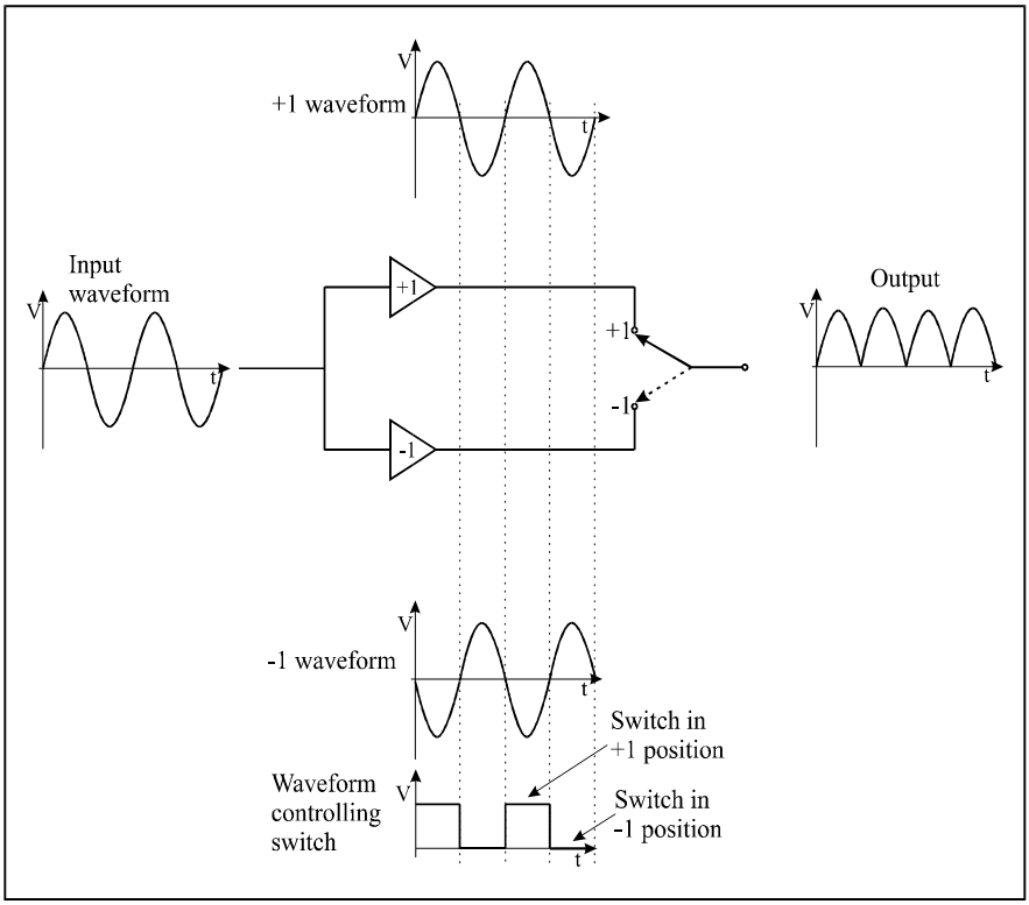

Figure 3: Full wave signal rectification

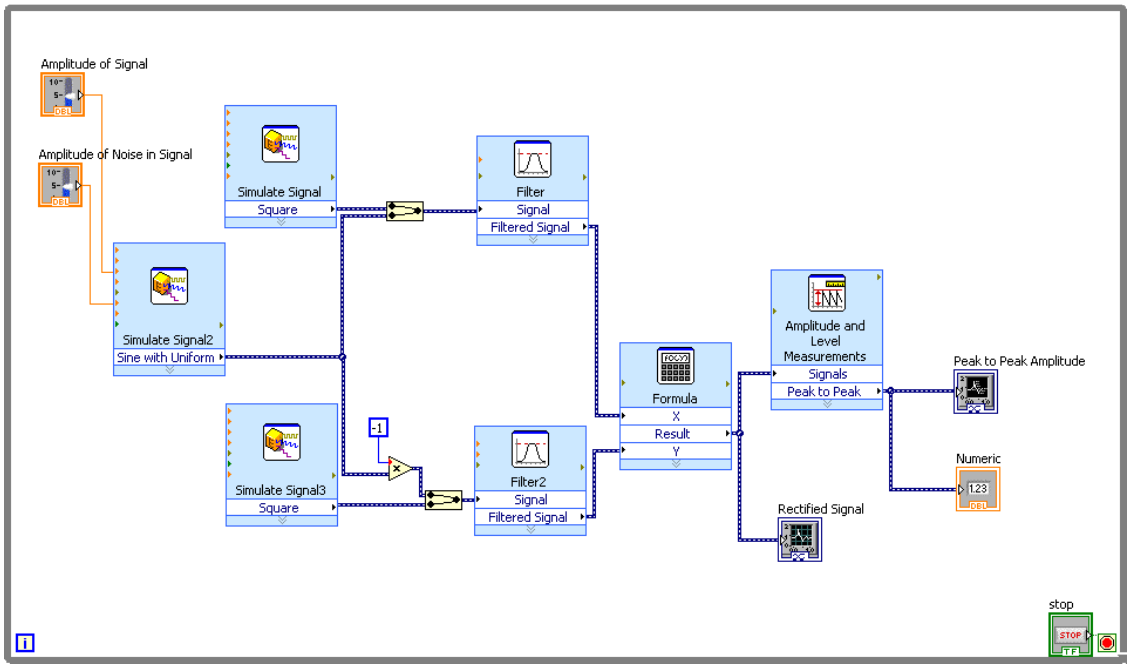

Figure 4: Square wave chopper + low-pass model block diagram

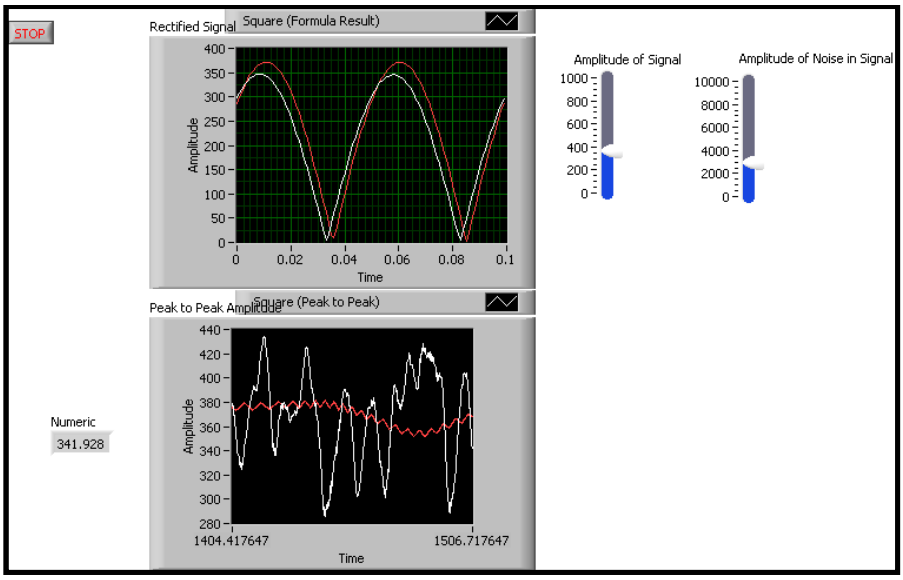

Figure 5: Square wave chopper + low-pass model front panel

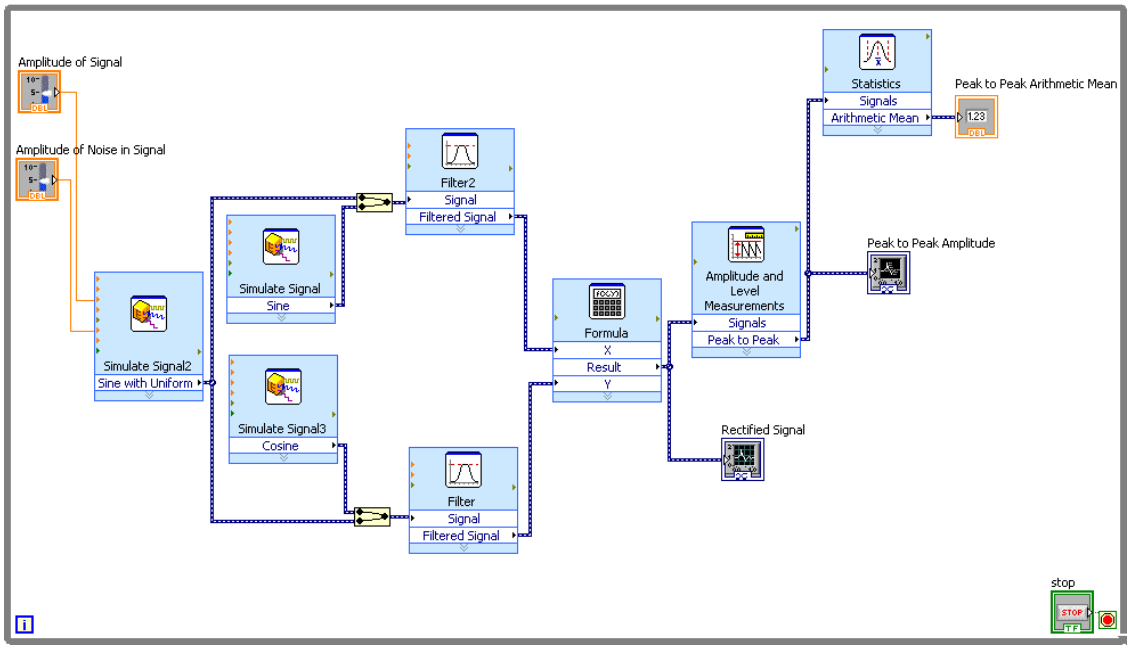

Figure 6: Sinusoidal wave chopper + low-pass model block diagram

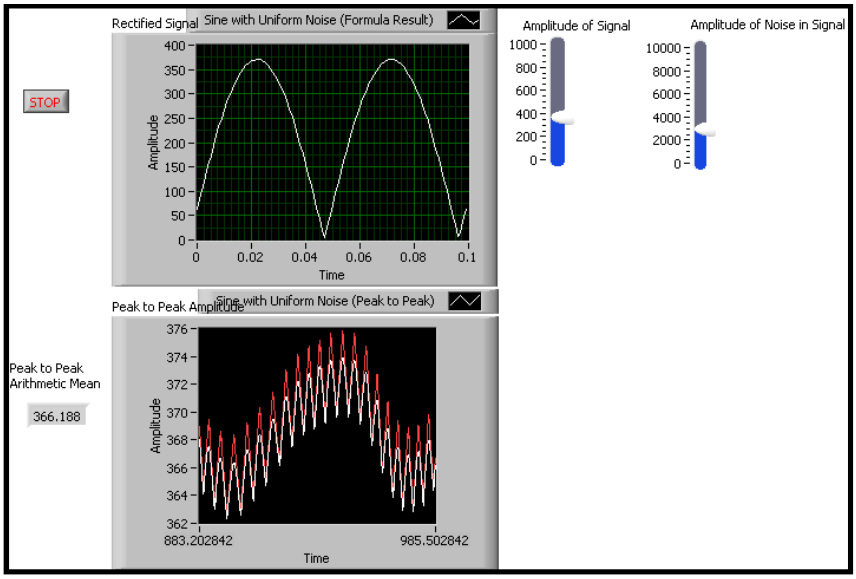

Figure 7: Sinusoidal wave chopper + low-pass model front panel

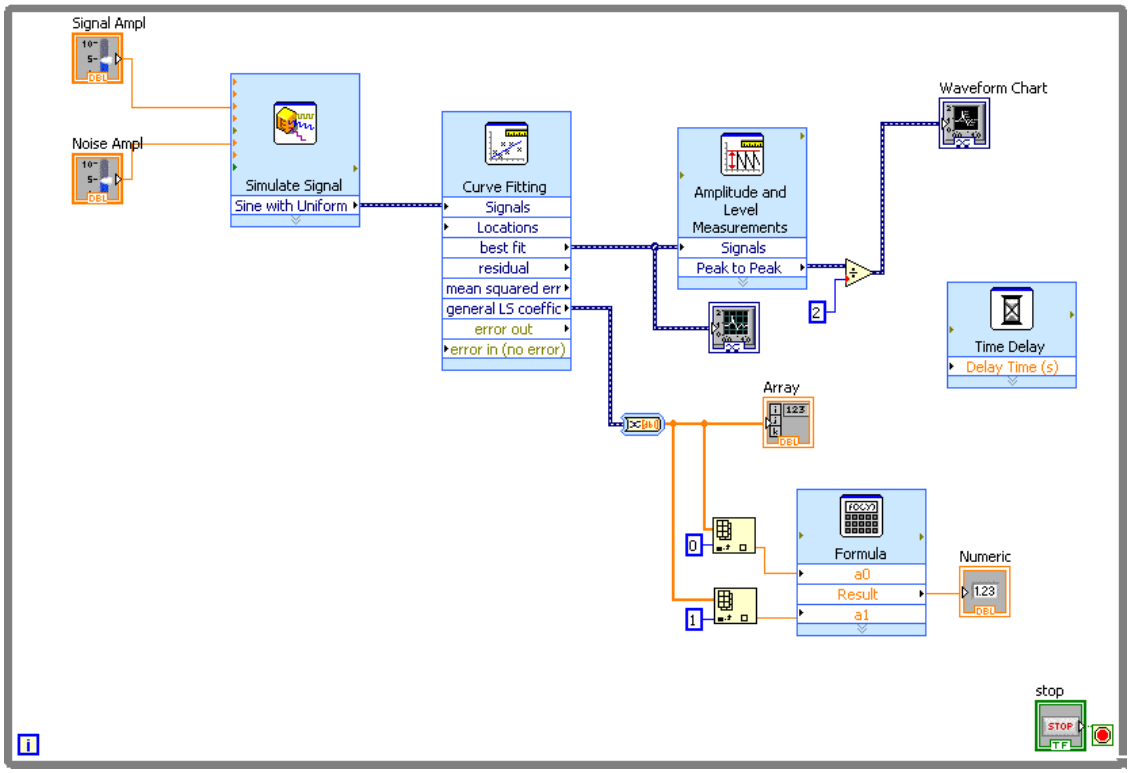

Figure 8: Curve fitting model block diagram

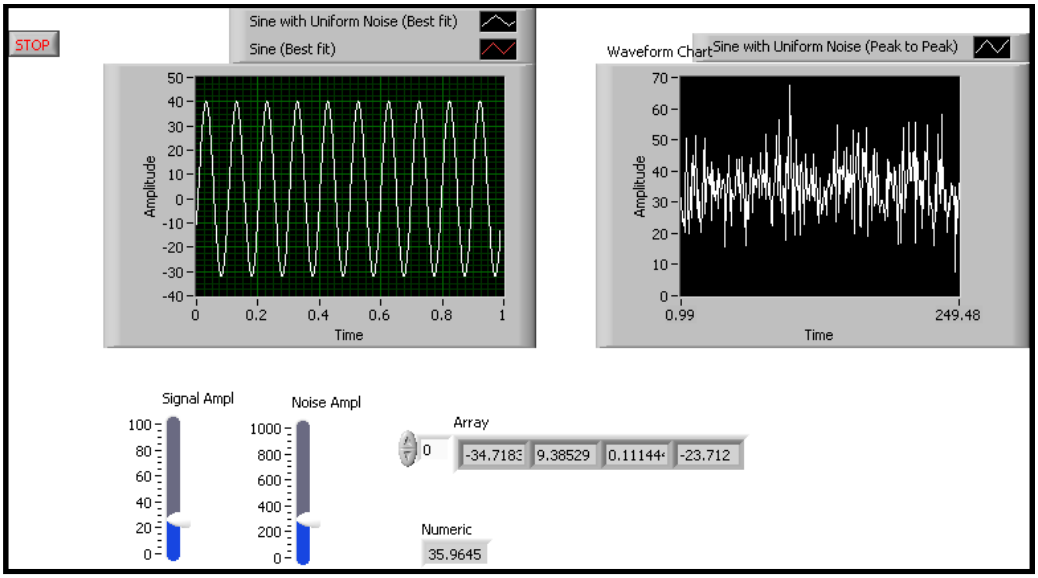

Figure 9: Curve fitting model front panel

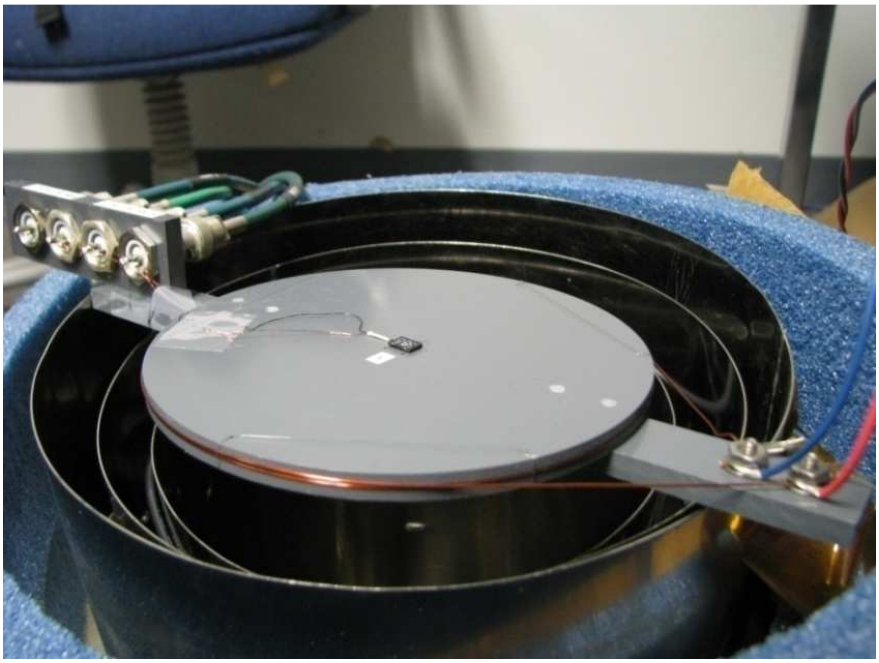

Figure 10: Magnetic Measurement System (supported by the nested magnetic shield)

Figure 11: Coil current source – Hewlett Packard E3610A

Figure 12: National Instruments PXI-1031 DC. Modules: PXI-8336, PXI-GPIB, PXI-6281

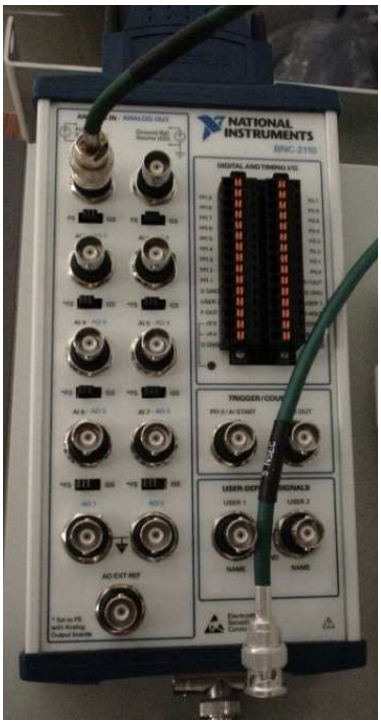

Figure 13: National Instruments BNC-2110

a)

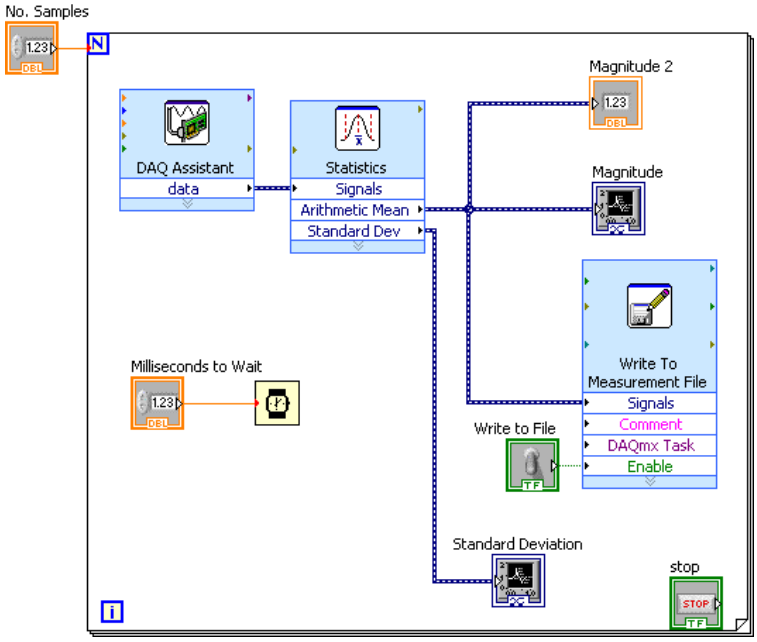

b)

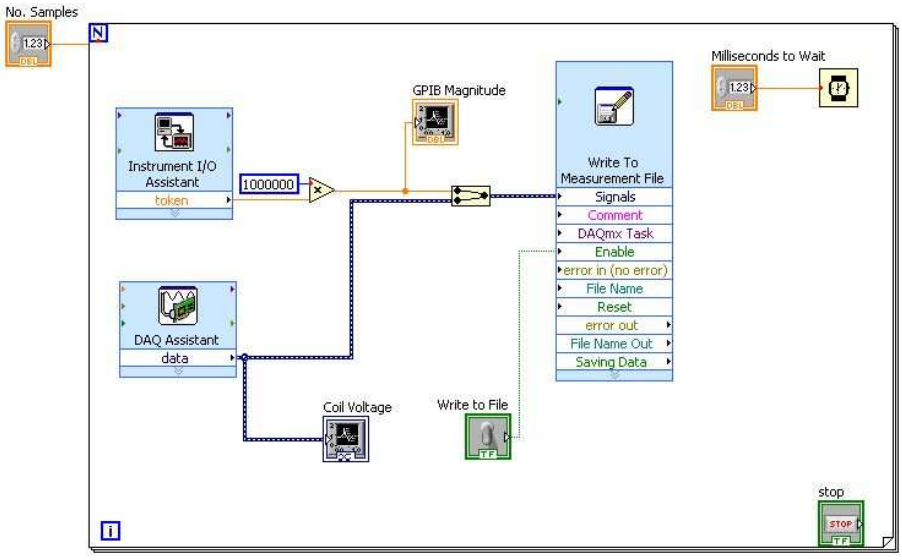

Figure 14: Typical LabVIEW data recording programs. a) Analog voltage reading and recording.

B) Analog and GPIB voltage reading and recording.

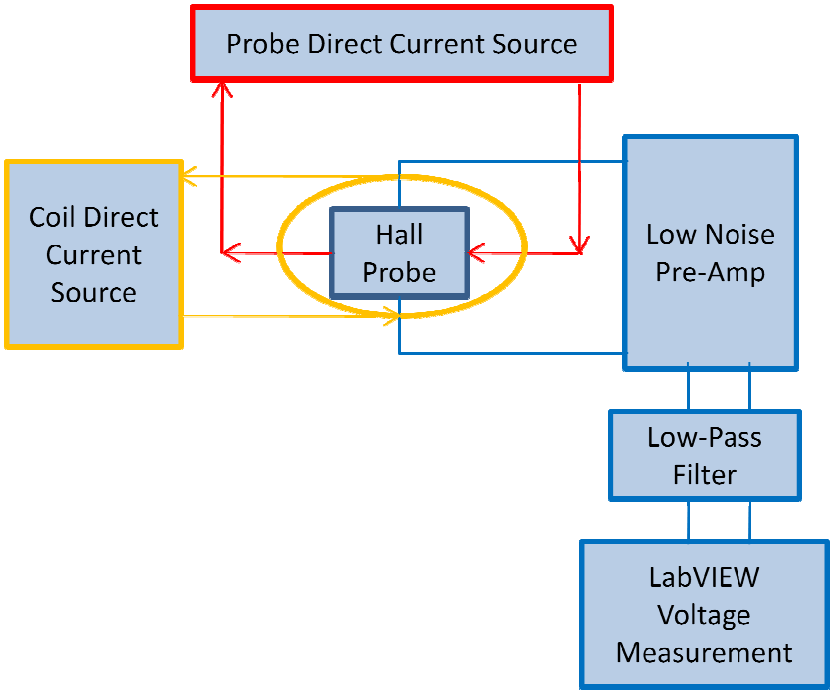

Figure 15: DC probe excitation setup– Sensitivity and noise level measurement

Figure 16: Probe DC power source – Keithley 2400 SourceMeter

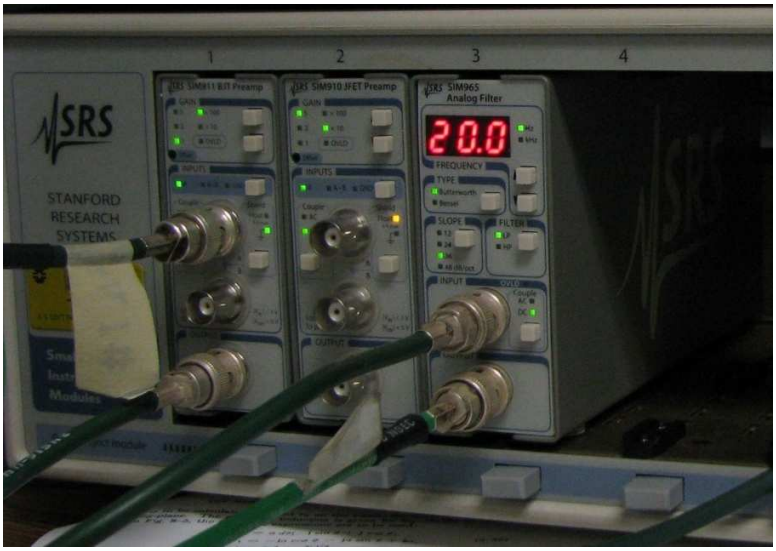

Figure 17: Stanford Research Systems – SIM 911 BJT Preamp and SIM 965 Analog Filter

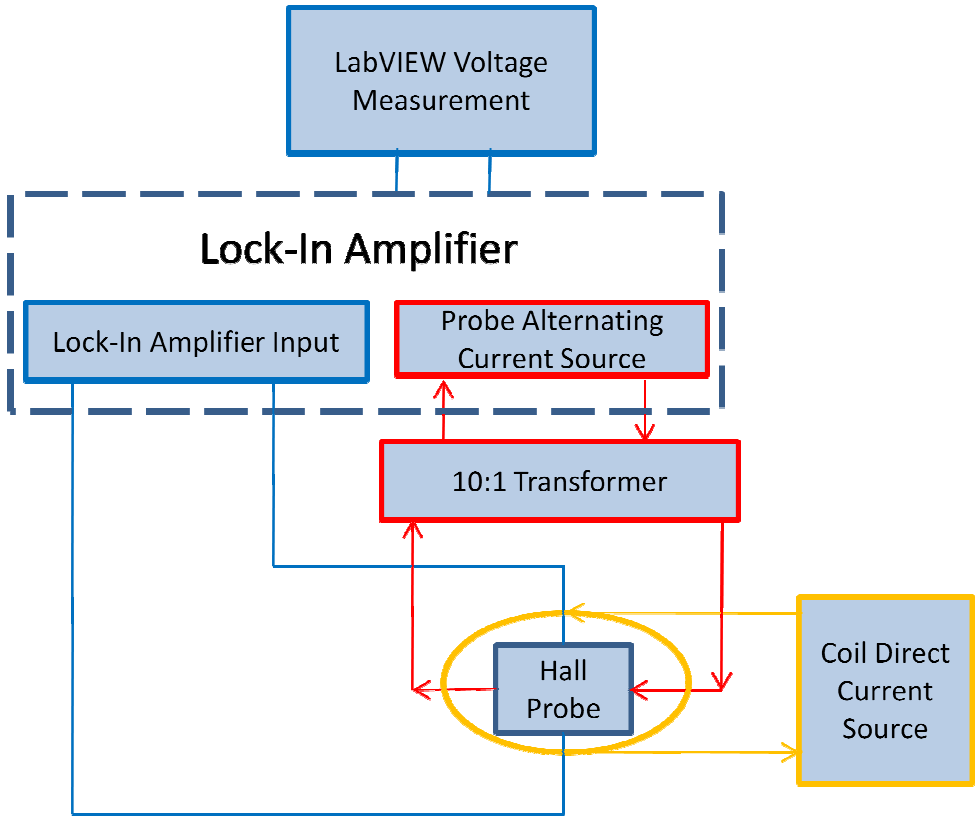

Figure 18: AC probe excitation setup – Sensitivity and noise level measurement

Figure 19: Signal Recovery's 7265 Lock-In Amplifier and a 10:1 transformer

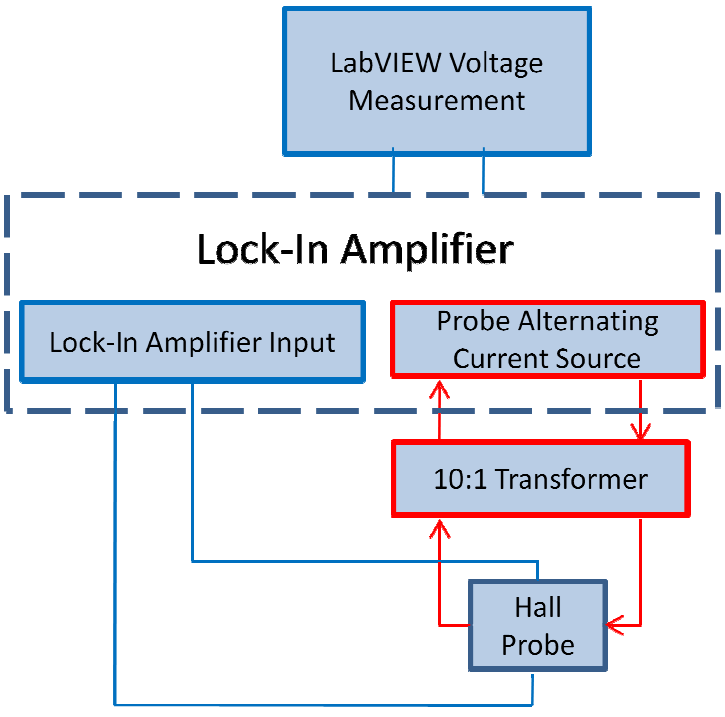

Figure 20: AC Source Noise Frequency Response Setup

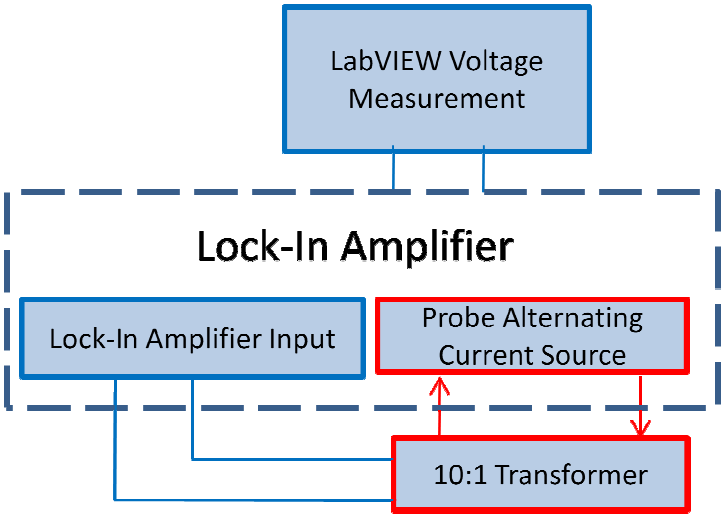

Figure 21: Transformer operation versus frequency setup

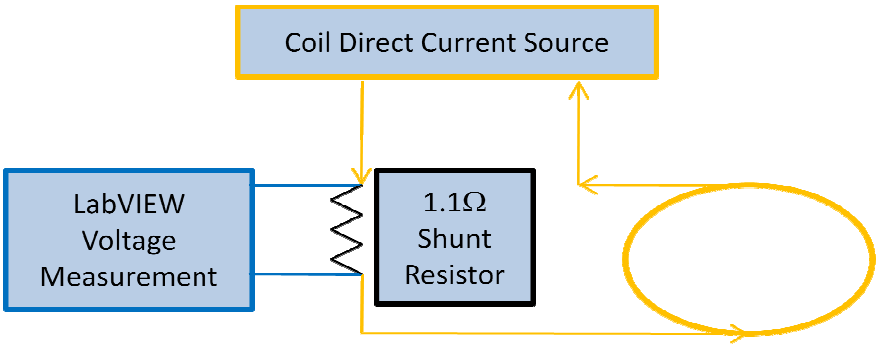

Figure 22: Coil current noise analysis setup

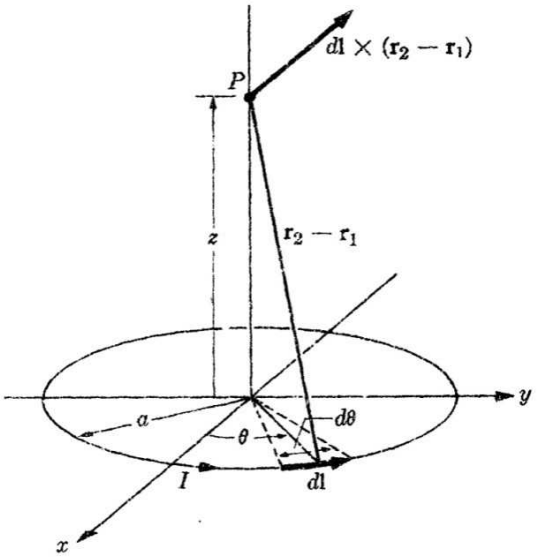

Figure 23: Magnetic field at a distance z from the center of a circular conducting ring of radius a, carrying a steady current I

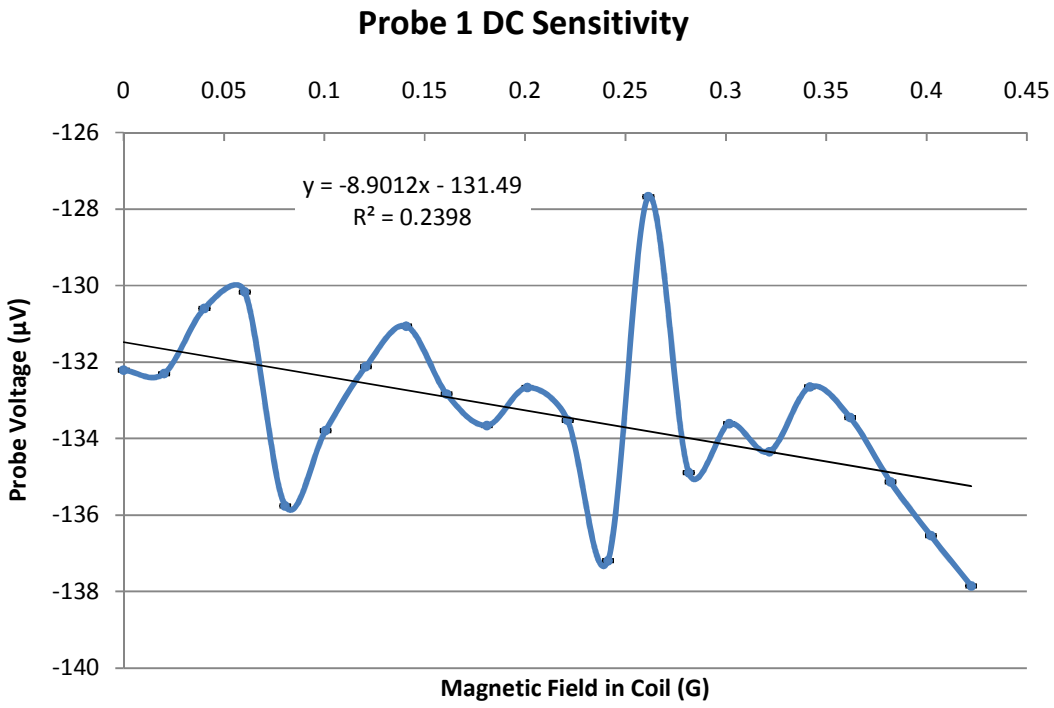

Figure 24: Probe 1 DC sensitivity with no filter

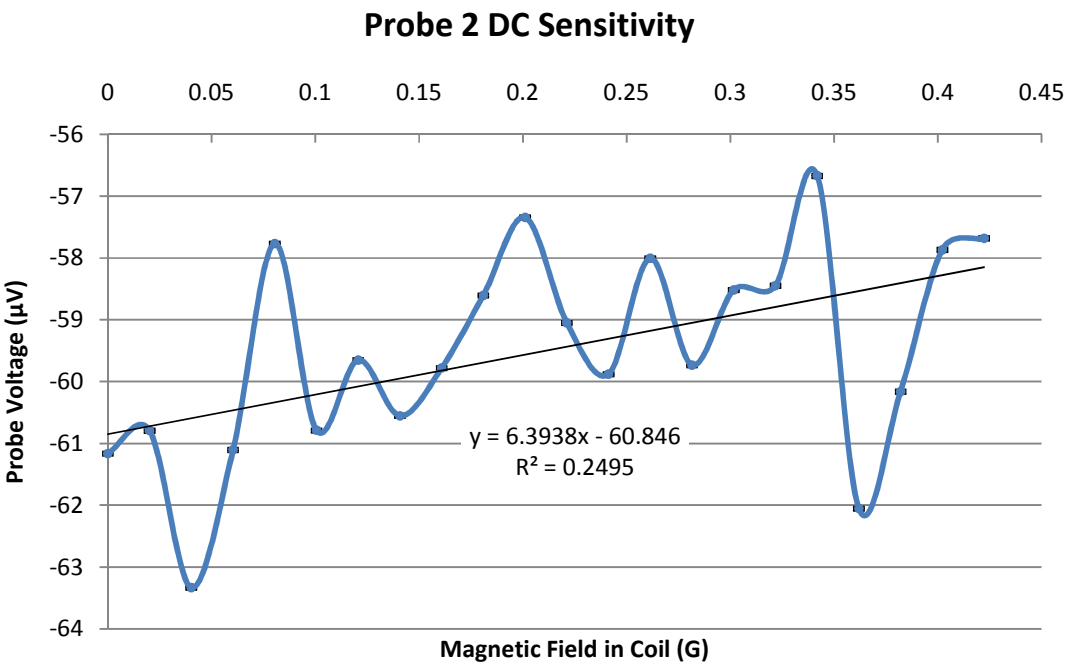

Figure 25: Probe 2 DC sensitivity with no filter

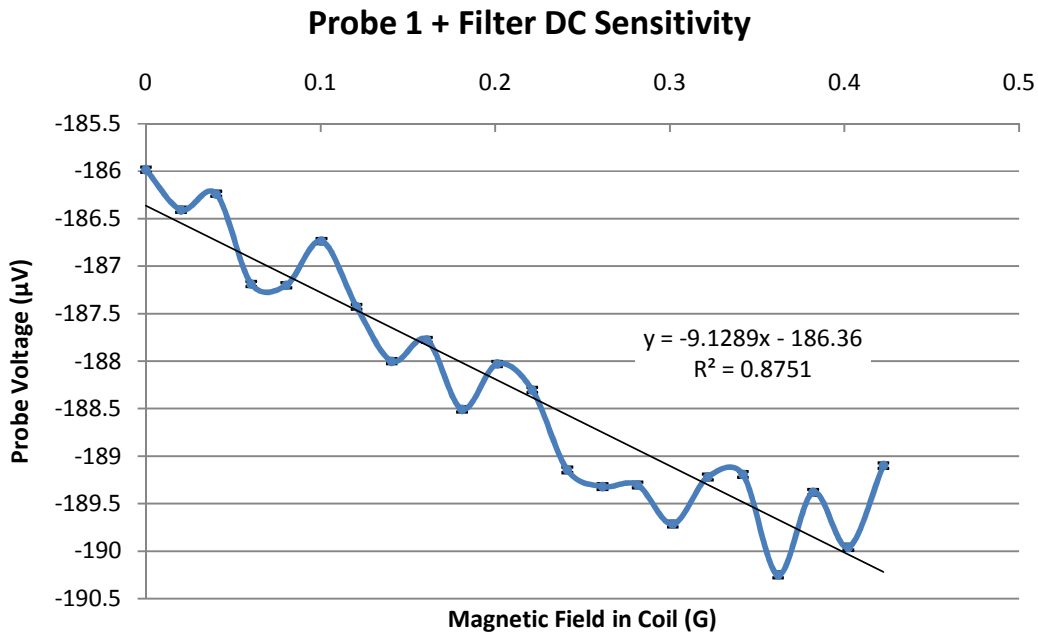

Figure 26: Probe 1 DC sensitivity with Butterworth filter

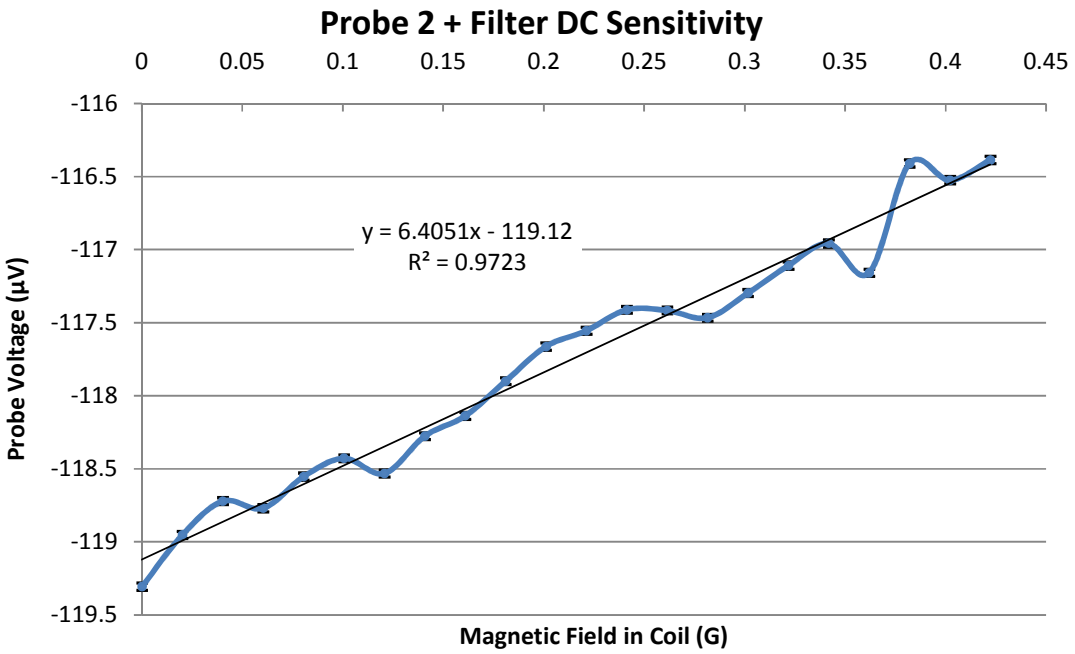

Figure 27: Probe 2 DC sensitivity with Butterworth filter

	Probe Sensitivity (µV/G)	Noise Level for Linear Fit (G)	Noise Level for Voltage Samples (G)
Probe 1 No-Filter	8.438	0.245	0.352
Probe 2 No-Filter	6.394	0.227	0.311
Probe 1 Lo-Pass Filter (20 Hz)	9.129	0.0493	0.00344
Probe 2 Lo-Pass Filter (20 Hz)	6.045	0.0220	0.00399

Table 1: DC probe excitation sensitivity & noise level results

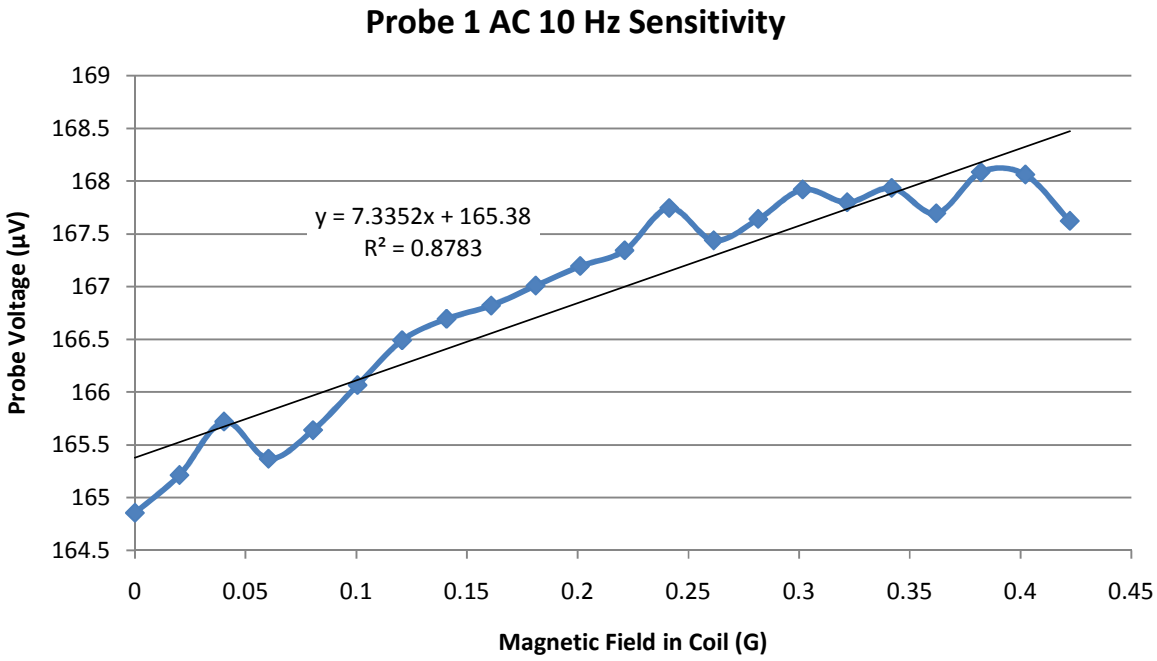

Figure 28: Probe 1 AC excitation at 10Hz – Sensitivity

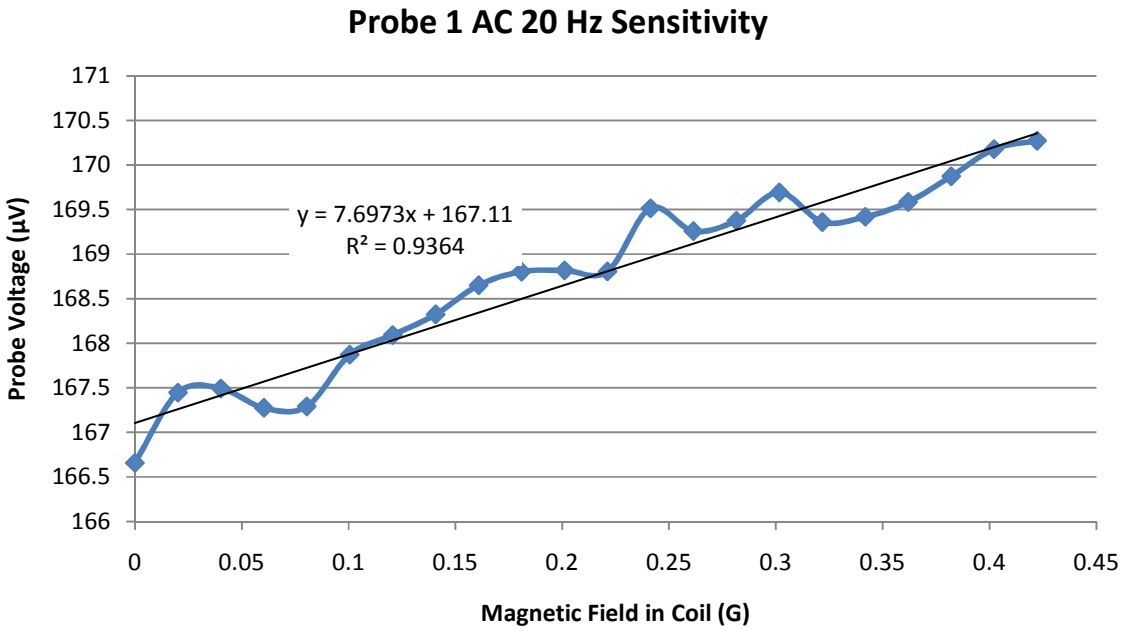

Figure 29: Probe 1 AC excitation at 20Hz – Sensitivity

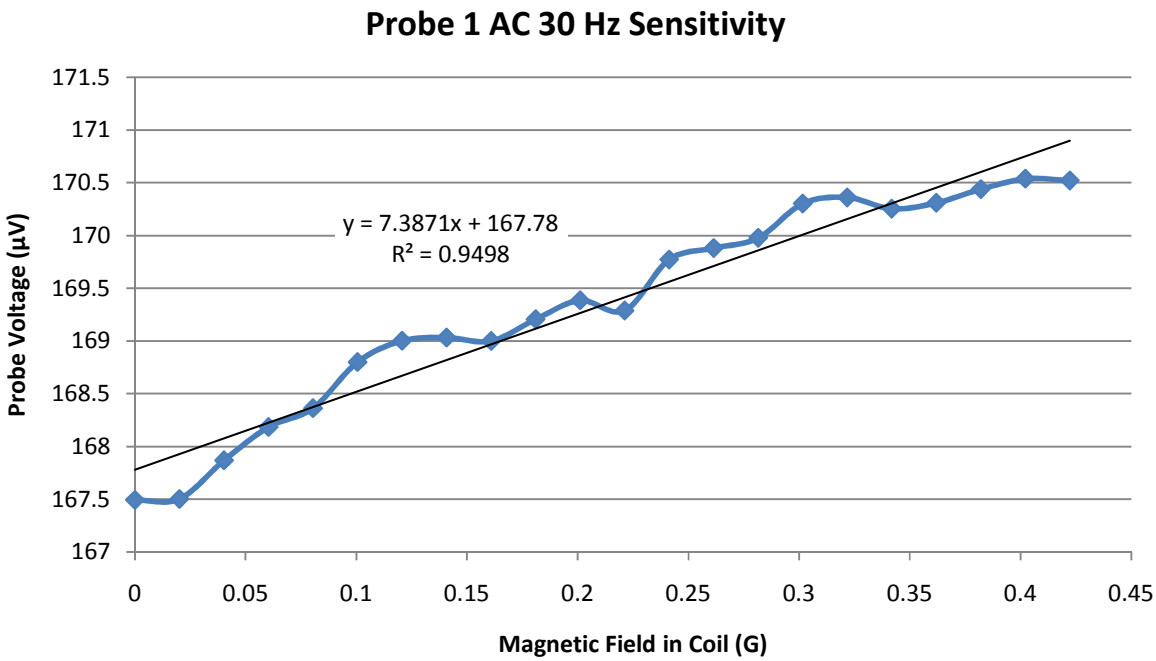

Figure 30: Probe 1 AC excitation at 30Hz – Sensitivity

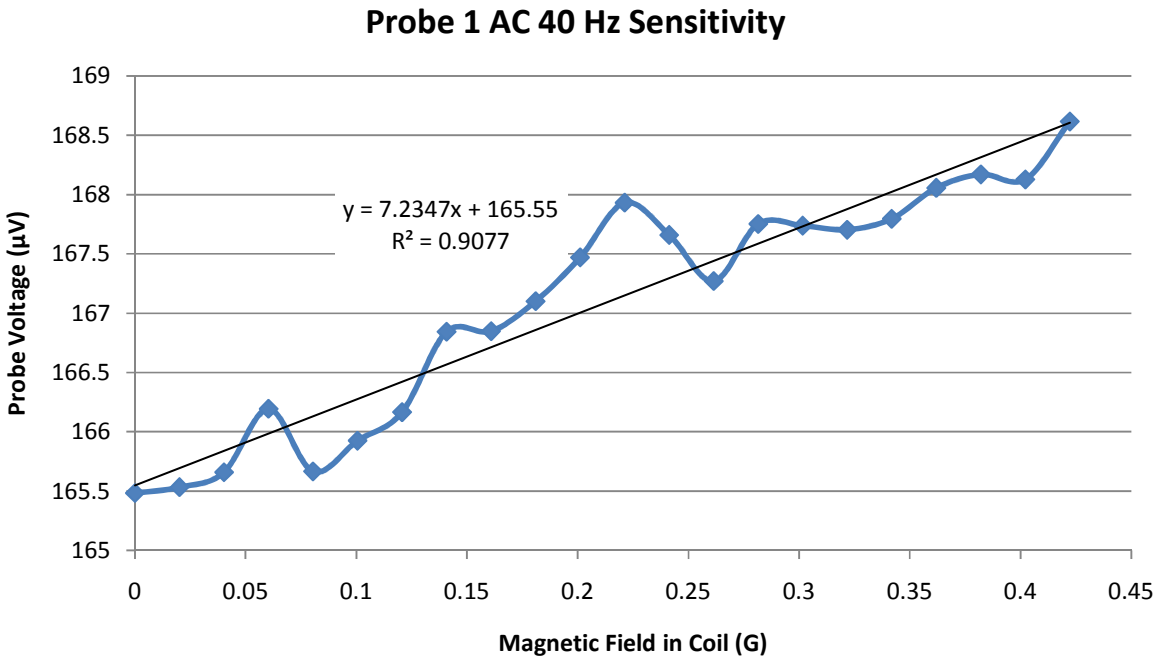

Figure 31: Probe 1 AC excitation at 40Hz – Sensitivity

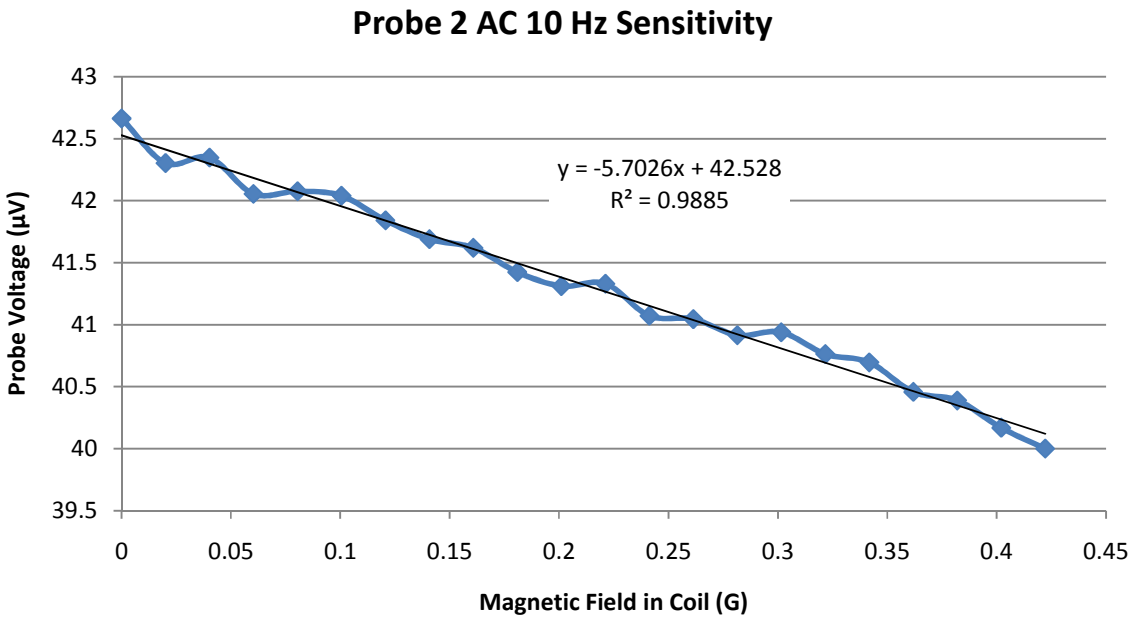

Figure 32: Probe 2 AC excitation at 10Hz – Sensitivity

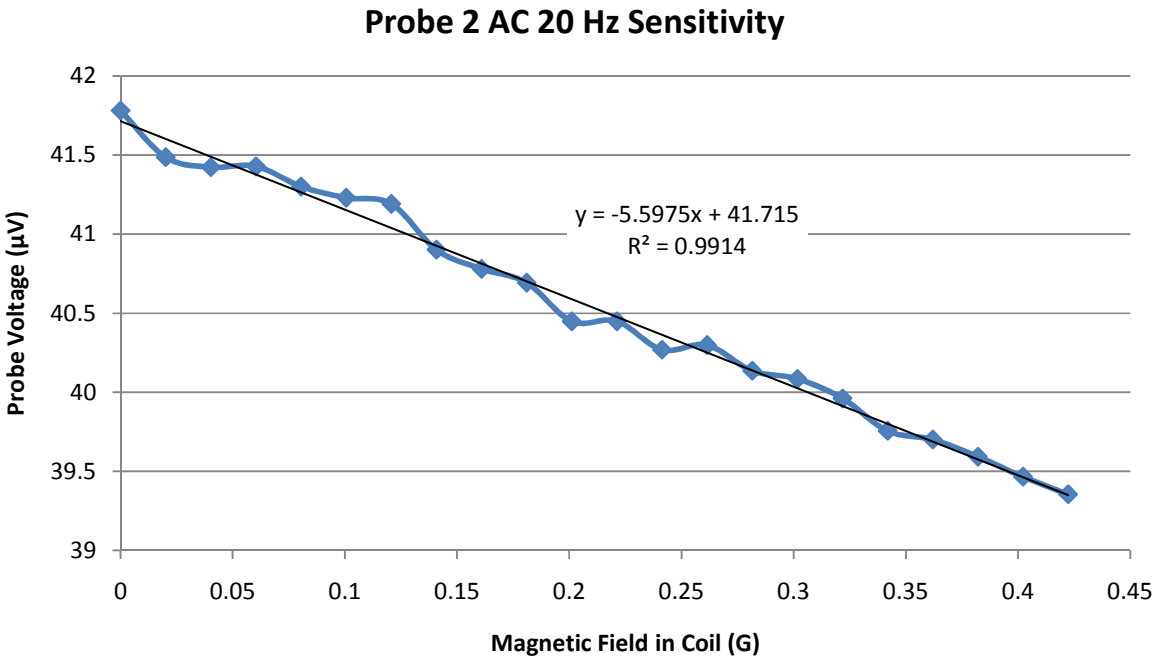

Figure 33: Probe 2 AC excitation at 20Hz – Sensitivity

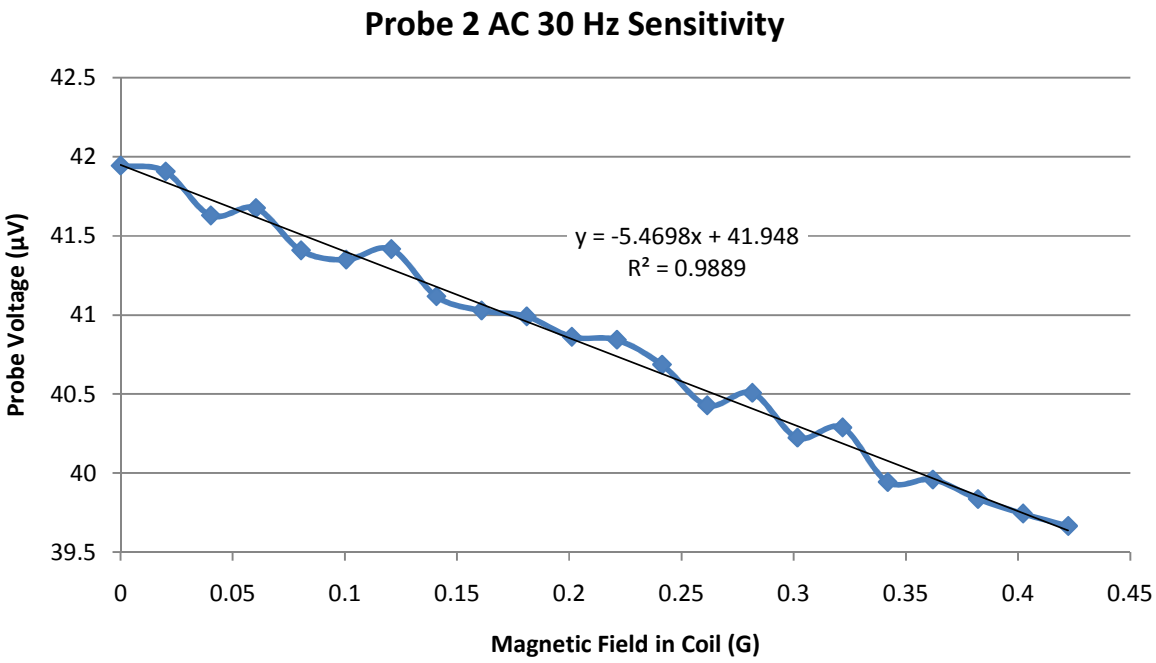

Figure 34: Probe 2 AC excitation at 30Hz – Sensitivity

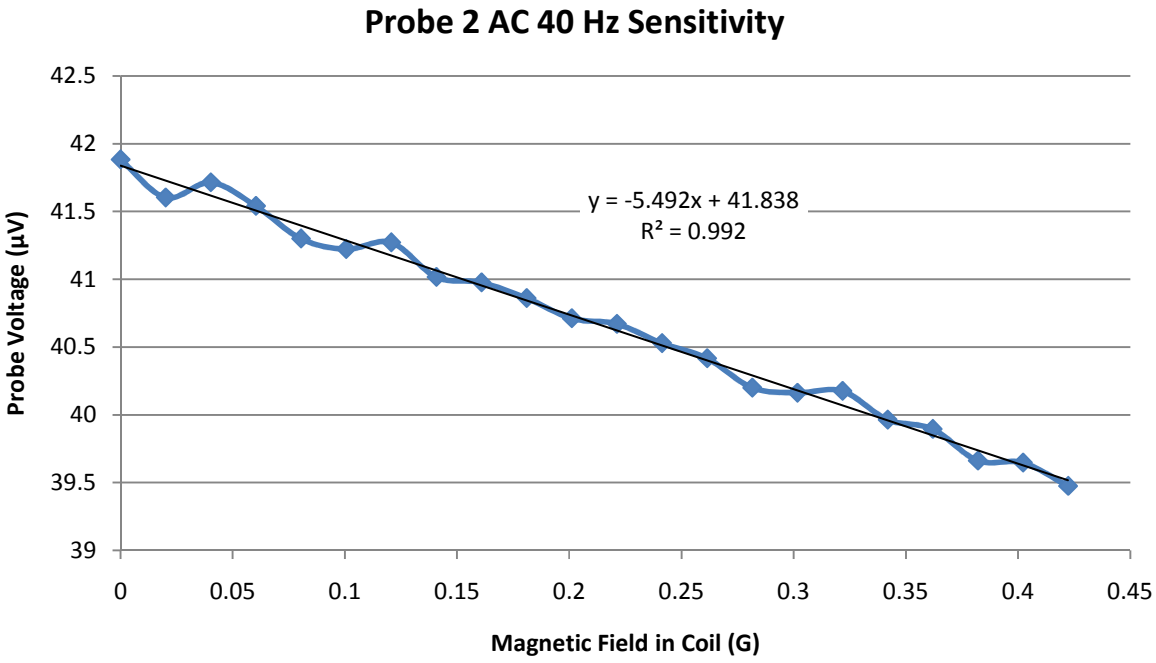

Figure 35: Probe 2 AC excitation at 40Hz – Sensitivity

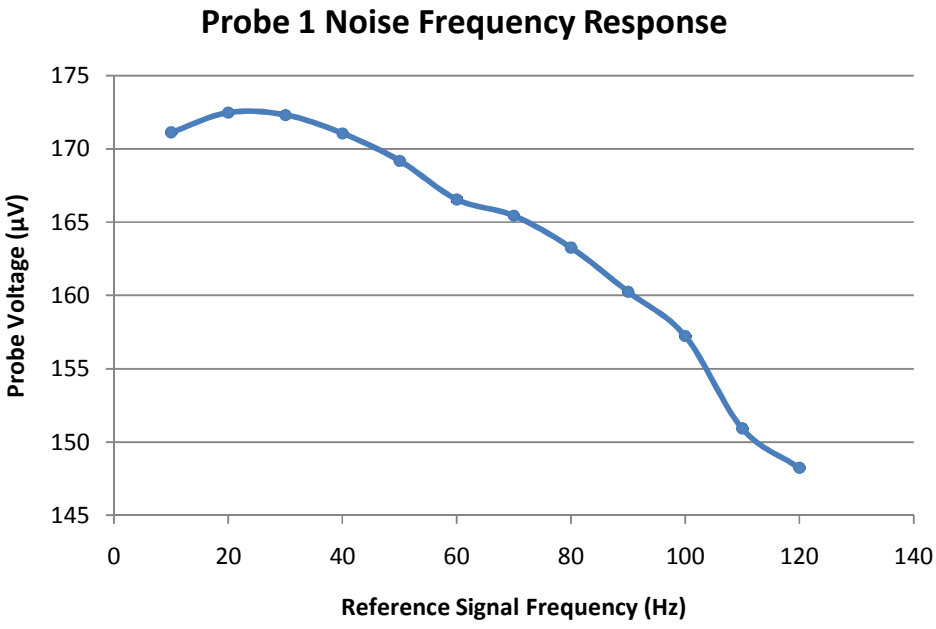

Figure 36: Probe 1 AC noise frequency response curve

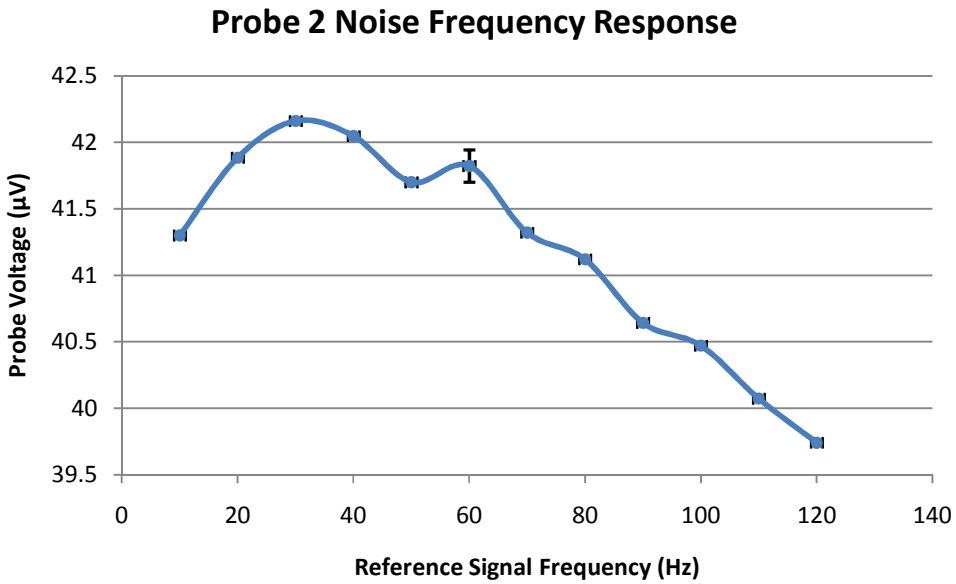

Figure 37: Probe 2 AC noise frequency response curve

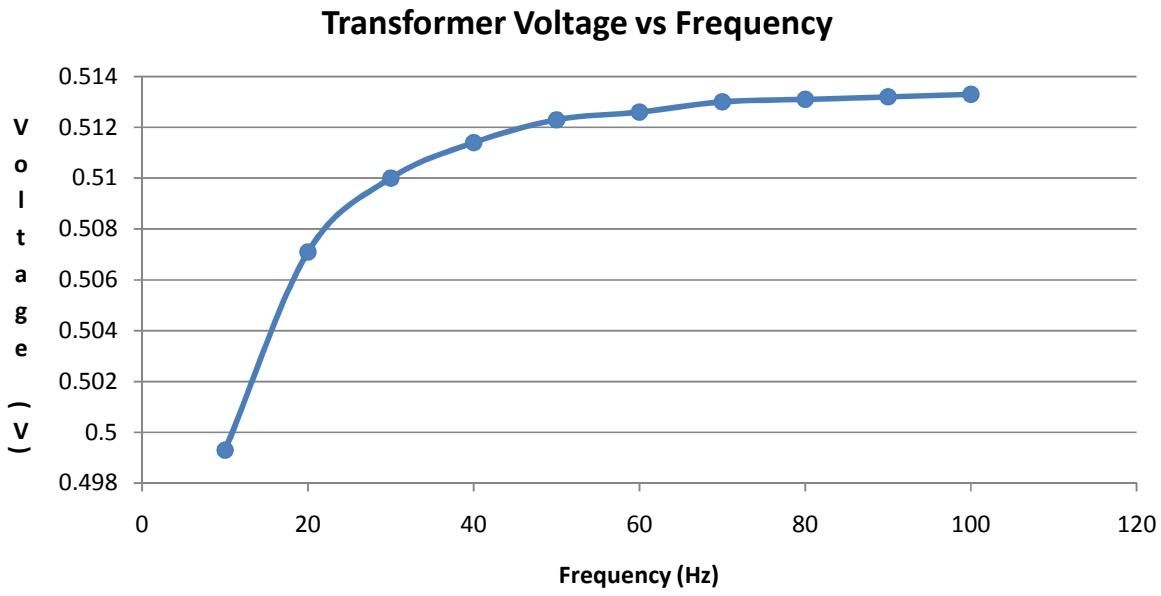

Figure 38: Transformer operation versus frequency

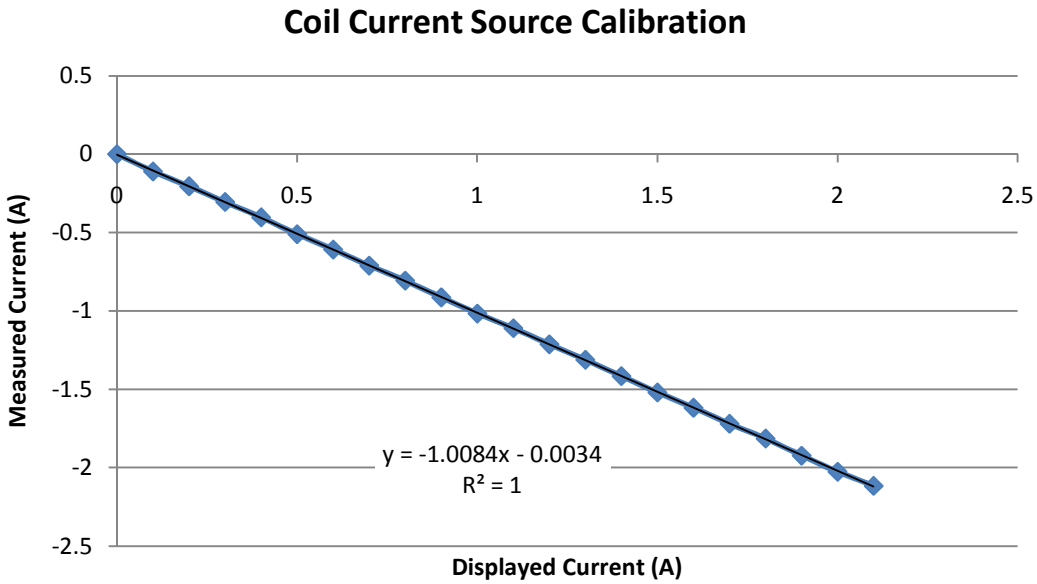

Figure 39: Coil current source noise level

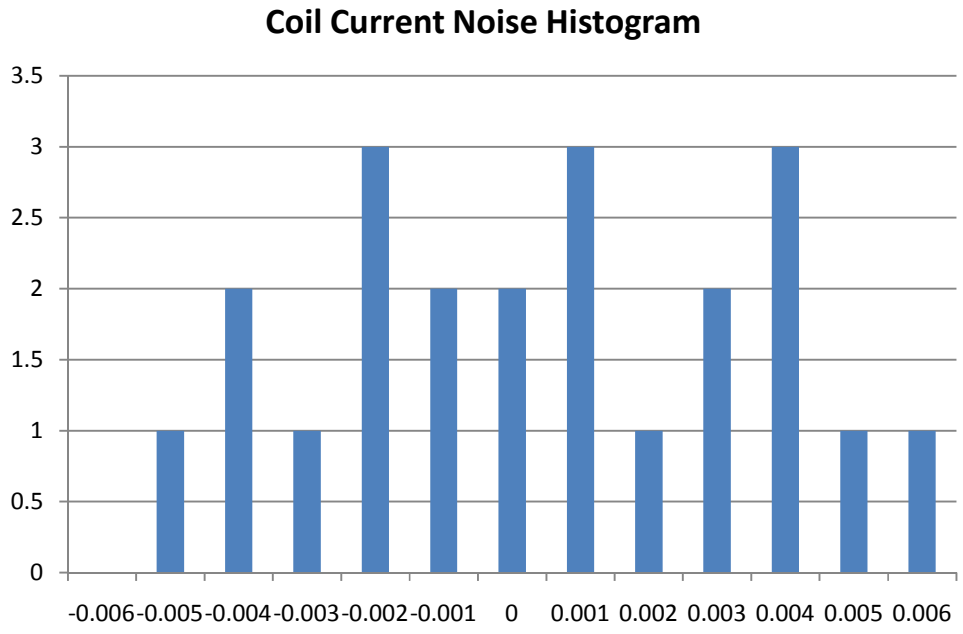

Figure 40: Coil current source noise histogram

	Probe Sensitivity (µV/G)	Linear Fit Noise Level (G)	Voltage Samples Noise Level (G)
AC Probe 1	7.387	0.0300	0.00181
AC Probe 2	5.470	0.0138	0.00240
DC Probe 1+Filter	9.129	0.0493	0.00344
DC Probe 2+Filter	6.045	0.0220	0.00399

Table 2: Results Summary